



Measurement of the $t\bar{t}$ Production Cross-section at $\sqrt{s} = 1.96$ TeV in Dilepton Final States

The DØ Collaboration
(Dated: March 26, 2004)

A measurement of the $t\bar{t}$ production cross-section at $\sqrt{s} = 1.96$ TeV from events manifesting in dilepton final states: ee +jets (156.3 pb^{-1}), $\mu\mu$ +jets (139.6 pb^{-1}) and $e\mu$ +jets (142.7 pb^{-1}), is presented. The preliminary cross-sections obtained for each of the dilepton channels and the combined cross-section are:

$$\begin{aligned} ee &: \sigma_{t\bar{t}} = 19.1_{-9.6}^{+13.0} \text{ (stat)} \quad {}_{-2.6}^{+3.7} \text{ (syst)} \pm 1.2 \text{ (lumi) pb;} \\ \mu\mu &: \sigma_{t\bar{t}} = 11.7_{-14.1}^{+19.7} \text{ (stat)} \quad {}_{-5.0}^{+7.9} \text{ (syst)} \pm 0.8 \text{ (lumi) pb;} \\ e\mu &: \sigma_{t\bar{t}} = 13.1_{-4.7}^{+5.9} \text{ (stat)} \quad {}_{-1.7}^{+2.2} \text{ (syst)} \pm 0.9 \text{ (lumi) pb;} \\ \text{dilepton} &: \sigma_{t\bar{t}} = 14.3_{-4.3}^{+5.1} \text{ (stat)} \quad {}_{-1.9}^{+2.6} \text{ (syst)} \pm 0.9 \text{ (lumi) pb.} \end{aligned}$$

Preliminary Results for Winter 2004 Conferences

I. INTRODUCTION.

In $p\bar{p}$ collisions at the Tevatron at $\sqrt{s} = 1.96$ TeV the Standard Model top quark is expected to be dominantly produced via the strong interaction (85% by the $q\bar{q}$ annihilation and 15% by the gluon fusion process, respectively) in LO. Recent work has substantially increased the knowledge of higher order contributions [1, 2]. The measurement of this cross-section thus provides an important test of perturbative QCD which predicts a cross-section of approximately 7 pb.

The top quark is expected to be unique among the quarks in several aspects due to its large mass of approximately 175 GeV/ c^2 . Its decay proceeds on a timescale shorter than typical fragmentation timescales to a non-virtual W -boson and a b -quark. The final states, visible in the detector, are dictated by the the decay modes of the W -boson and the b -quark. Events in which both W 's decay leptonically are termed 'dilepton' events, those with one W decaying leptonically and the other to quarks are 'lepton+jets' events, and those with both W 's decaying to quarks are called 'all-jets' events. This paper considers $t\bar{t}$ events with dilepton final states based on a purely topological analysis, i.e. no b -tagging techniques are applied here.

II. DATA SET

The data sample used consists of data taken during the period between April 2002 and September 2003. In the ee -channel, runs are used in which tracking and calorimeter detector status is good. The other two analyses also require good performance of the muon system. Table I summarizes the total integrated luminosity of the data set for each analysis.

$\int \mathcal{L} \text{ (pb}^{-1}\text{)}$	ee	$e\mu$	$\mu\mu$
total	156.33	142.73	139.58

TABLE I: Integrated luminosity used in this analysis for each channel.

III. OBJECT IDENTIFICATION

The DØ detector is a large, multipurpose collider detector with a central tracking volume immersed in a 2 T solenoidal magnetic field, surrounded by a liquid-argon/uranium sampling calorimeter, and located inside a full coverage muon detector. These detectors provide excellent capabilities for the identification and measurement of electrons, jets, muons and neutrinos.

Electrons are identified as clusters in the electromagnetic layers of the calorimeter found within $\Delta R \equiv \sqrt{\Delta\phi^2 + \Delta\eta^2} = 0.4$ using the simple cone algorithm. These clusters are further required to be isolated from nearby hadronic energy, to satisfy a loose shower shape selection, and to satisfy a loose match to a central track. In the final selection a multiparameter likelihood discriminant is used which compares the probabilities of a particular candidate to be an electron or background (i.e. a highly electromagnetic jet), $\mathcal{L}_e = \prod \frac{p_{S,i}}{p_{S,i} + p_{B,i}}$, where $p_{S,i}$ and $p_{B,i}$ are the probabilities to be signal or background, respectively, given a measurement i . This likelihood is constructed from the distributions in data of the electromagnetic energy fraction, shower shape, spatial track match, E/p , distance of closest approach of the track to the primary vertex, and two tracking isolation variables (one in a narrow cone, and one in a wide cone). Both central ($|\eta| < 1.1$) and forward ($1.5 < |\eta| < 2.5$) electrons are utilized for the analyses. Energy scale corrections are derived from observing electrons from Z decays and using the known Z mass as a constraint.

Muons are comprised of a track segment in the inner muon layer matching a segment formed from hits in the outer two muon layers. A central track must also match the muon track, and the overall track $\chi^2_{track} < 4$. Timing cuts are applied based on muon scintillator signals which reject cosmic ray muons. All muons must be found in $|\eta| < 2.0$. Muons supposedly originating from W (or Z) decay are identified using two isolation criteria: energy deposition near the muon as measured in the calorimeter, and an analogous measure as observed in the central tracker. The significance of the distance of closest approach of the muon track from the primary event vertex ($|dca|/\sigma_{dca}$) is required to be small, i.e. non-indicative of a heavy flavour decay muon.

Jets are reconstructed using an iterative algorithm integrating energy observed in the calorimeter in a cone with radius, $\Delta R = 0.5$. These jets are required to be in the region $|\eta| < 2.5$. Cuts on the longitudinal energy deposition profile and the energy fraction of the leading cell are applied which efficiently discriminate between real jets and those arising from hot calorimeter cells. The energy of jets is corrected after reconstruction based on studies of response (R),

showering (S), and underlying event, extra interactions and noise (O) according to $E = \frac{E^{meas} - O}{R * S}$. These corrections bring the jet energy scale to the level of the particles that are incident on the calorimeter inner wall. An equivalent correction is derived for Monte Carlo events to bring them to the same level as the data. A further correction for b -jets is applied when a soft muon is found in a jet. This correction compensates for all of the muon energy, and all of its corresponding neutrino energy to be unobserved in the calorimeter.

A global event quantity, termed missing transverse energy, or \cancel{E}_T , is calculated to give an indication of neutrinos of substantial P_T in an event. The transverse energy in the calorimeter towers is vectorially summed. The \cancel{E}_T is then the negative of this sum and implies an unmeasured imbalance in the event due to a neutrino. The outer, coarse hadronic layer of the calorimeter is omitted in this sum, unless such energy comprises a reconstructed jet. The change in each electron or jet P_T due to response corrections as described above is vectorially added into the \cancel{E}_T , as are any observed muons.

The event primary vertex is calculated from reconstructed central tracks. Events are rejected if this vertex is not found to be within $|z| < 60.0$ cm of the center of the detector, or if it is not calculated from at least 3 tracks.

The $D\bar{O}$ trigger is a three-level trigger system. Level 1 is a hardware trigger, while level 2 and 3 are software triggers. The dilepton triggers require both leptons at the first trigger level, and one or two leptons at the third trigger level. The dimuon channel also has a refined muon requirement at Level 2, including track information. Typical trigger efficiencies are between 91.7% ($\mu\mu$) and 95.2% (ee).

IV. MONTE CARLO SIGNAL AND BACKGROUND SAMPLES

The $t\bar{t}$ signal expectations are determined from a full Monte Carlo (MC) simulation of top-antitop events. This simulation utilizes events generated at $\sqrt{s} = 1.96$ TeV with the ALPGEN 1.2 [3] matrix element generator assuming a top mass of 175 GeV/ c^2 and the parton distribution function set CTEQ 6.1M [4]. These events are processed through PYTHIA 6.2 [5] to provide higher order QCD evolution (i.e. gluon radiation and fragmentation) and short lived particle decays. EvtGen is used to model the decays of b hadrons. The W 's are both decayed to a lepton-neutrino pair, including all τ final states. These events are processed through a full detector simulation providing tracking hits, calorimeter cell energy and muon hit information. Extra interactions are added to all events subject to Poisson statistics given the instantaneous luminosities typically observed in the run. The same reconstruction is applied to data and Monte Carlo events.

Although most of the main backgrounds are studied using data, considerable resources are devoted to event simulations. The main physics background ($Z/\gamma^* \rightarrow lljj$ ($l = e, \mu, \tau$)), is generated using ALPGEN followed by PYTHIA. To evaluate the $Z/\gamma^* \rightarrow \mu\mu$ and $Z/\gamma^* \rightarrow \tau\tau$ background before the jet requirement is applied, PYTHIA samples are used. The WW background is studied using ($WW \rightarrow lljj$, and $WW \rightarrow ll$ with ($l = e, \mu, \tau$) using ALPGEN followed by PYTHIA. In each case, τ 's are forced to decay to either electrons or muons. In case of $Z/\gamma^* \rightarrow \tau\tau$, the $D\bar{O}$ measurement (uncorrected for photon exchange and photon- Z interference) [6] is used. In case of $WW \rightarrow ll$, the next-to-leading-order (NLO) calculation [7] is used, instead of the leading-order (LO) ALPGEN cross-section, which represents an increase of 35% with respect to LO. For consistency, in the case of ($WW \rightarrow lljj$), the LO ALPGEN cross-section is scaled up by 35% and a systematic uncertainty is included since no such NLO calculation is available for that process.

When utilizing simulated samples for analysis, additional smearing of the momenta of muons, electrons and jets is performed according to the observed resolutions in data. Correction factors to Monte Carlo efficiencies accounting for differences in, for instance, lepton identification efficiencies in data and Monte Carlo are also applied.

V. DILEPTON ANALYSIS

The signatures for dilepton final states include two oppositely charged, isolated high P_T leptons, two high P_T jets, and large missing E_T . The selection is $P_T^{l2} > 15$ GeV (20 GeV for 'ee'), $P_T^{j1,2} > 20$ GeV, and $\cancel{E}_T > 25$ GeV. The like-flavored channels tighten the missing \cancel{E}_T cut to 35 GeV and reject all events with M_{ll} near the Z mass to suppress the Z/γ^* background. The total transverse energy, as calculated from the scalar sum of the jet P_T 's is termed H_T . The total transverse energy across channels has been redefined to include the leading lepton, whether it be a muon or an electron, and is required to be $H_T^{leading\ lepton} > 120$ (140) GeV in $\mu\mu$ ($e\mu$) channel, respectively.

A. Physics Backgrounds

Background processes which can produce the full dilepton signature (two leptons, two jets, significant missing E_T) are quite rare. Decays of Z/γ^* to two τ 's which decays subsequently to electrons or muons suffer from the low branching ratio of two taus to two lighter leptons, as well as soft lepton and neutrino spectra. Diboson production, that of WW being the most important because it looks leptonically much like the leptonic side of top events, suffers from a very low cross section. As with all top backgrounds, higher numbers of produced jets further suppress these backgrounds relative to top.

In the three dilepton channels, these two backgrounds are estimated from the MC samples described above. Both backgrounds are determined to be small. The effects of uncertainties in lepton and jet resolutions, jet energy scale, and data to MC scale factors are estimated as part of the systematic uncertainty for each background.

B. Missing E_T Instrumental Backgrounds

The primary instrumental background arises from fake \cancel{E}_T in $Z/\gamma^* \rightarrow ee, \mu\mu$ events. Detector resolutions can give rise to observed E_T imbalances in events which look like evidence of neutrinos. A contribution also comes from QCD multijet production where electrons are faked in addition to the \cancel{E}_T , or a heavy flavor decay gives rise to a μ and \cancel{E}_T . In the dielectron analysis, the estimate of this background is obtained solely from data. A sample is defined with two high P_T electromagnetic clusters which each satisfy the isolation requirement plus a moderate shower shape requirement. Such a sample is dominated by photons or π^0 jets yielding clean photon-like behavior in the calorimeter. There is negligible presence of events with real \cancel{E}_T . The \cancel{E}_T performance of these events is compared to that of the sample with tight electron requirements in the low to medium \cancel{E}_T range, as well as a fully smeared $Z \rightarrow ee$ Monte Carlo over the whole spectrum, to ensure a good description of the behavior seen in Z events in data. The ratio of the number of events passing the \cancel{E}_T selection compared to the number of events failing it is measured in this sample, and then multiplied by the number of tight dielectrons failing the \cancel{E}_T cut, yielding an estimate of the number of events with tight electrons passing the \cancel{E}_T selection (the \cancel{E}_T fake rate). This estimate is performed in two dielectron invariant mass bins of $M_{ee} < 60$ GeV, and $M_{ee} > 130$ GeV. A systematic uncertainty on the \cancel{E}_T faking probability is assigned based on its sensitivity to changes in electron identification cuts.

The dimuon channel fake \cancel{E}_T background arises solely from the Z/γ^* process and is estimated from fully smeared Z/γ^* Monte Carlo in the same two dilepton invariant mass bins as described for the dielectron channel. In this channel, fake high missing E_T is much more prevalent from the degrading momentum resolution from high P_T tracks. Substantial work has been invested to understand these resolutions and bring the Monte Carlo into agreement with data.

C. Lepton Instrumental Backgrounds

Two more effects can cause events which are not top-like to satisfy our event selection criteria. Electrons can be mimicked by photons or jets which fragment to a leading π^0 which then acquire a track due to overlap with a nearby charged hadron or from photon conversion in the tracking volume. Non-isolated muons from jet fragmentation products or quark decay can occasionally appear isolated.

Remaining fake lepton backgrounds are estimated similarly for all three dilepton analyses. This involves measuring the rate for a non-isolated muon to appear isolated, or for an electromagnetic jet to fake a tight electron. In the electron-muon and dielectron cases, samples are selected which satisfy the signal trigger and which contain two electromagnetic clusters (ee case) or a muon and an electromagnetic cluster ($e\mu$ case). For the dielectron treatment, the invariant mass of the two cluster pair is required to be < 75 GeV and one cluster is required to have no matching central track. In the electron-muon case, the muon is required to be nonisolated. These requirements remove contributions from real leptons from Z/γ^* production. For the dimuon analysis, a sample of events is selected containing one muon which passes the signal trigger requirements and which is back-to-back with a b -tagged jet. In each sample, the rate for electromagnetic clusters or muons to pass the final identification and isolation criteria is measured.

The fake rate is applied to samples of events which satisfy all of the top selection criteria, except one electron (for ee or $e\mu$) or one muon (for dimuon) has its identification or isolation cuts omitted, respectively. These samples are then scaled by the relevant lepton faking probabilities. For the dielectron case, the small contribution for pure multijet production which is already accounted for in the \cancel{E}_T background, is subtracted to give the final estimate. For dimuons, a matrix approach is employed to separate the significant amount of signal from the loose-tight dimuon sample, and then the fake probability is applied to the non-signal portion.

D. Dielectron channel

The preselection of candidate events in the dielectron channel is based on the following requirements:

- primary vertex with $N_{trk} > 2$ and $|vtx_z| < 60$ cm
- 2 tight electrons (based electron ID likelihood) with track match, opposite electrical charge, electron track originates from primary vertex $|\Delta z(e, PV)| < 1$ cm
- electron trigger

Table II summarizes the cut flow at the various stages of the event selection after the preselection in the ee channel and Table III shows the final yield of background and signal events, the latter for the assumption of a $t\bar{t}$ production cross section of 7 pb.

Distributions of kinematic variables in the dielectron channel are shown in Appendix X.

Cut	Data	Total	Fakes	$Z/\gamma^* \rightarrow \tau\tau$	WW	$t\bar{t}$
$N_{ele}^{pT > 20} \geq 2 + \cancel{E}_T$ cut	17	14.29 ± 2.47	10.11 ± 2.35	0.22 ± 0.06	2.05 ± 0.73	$1.91^{+0.18}_{-0.21}$
$N_{jets} \geq 2$	6	$3.92^{+0.57}_{-0.60}$	1.89 ± 0.51	$0.19^{+0.08}_{-0.14}$	$0.27^{+0.16}_{-0.13}$	$1.57^{+0.18}_{-0.24}$
$N_{jets}^{pT > 20} \geq 2$	5	$2.59^{+0.36}_{-0.40}$	0.91 ± 0.30	$0.15^{+0.07}_{-0.12}$	$0.14^{+0.08}_{-0.07}$	$1.39^{+0.16}_{-0.22}$

TABLE II: Data, expected signal and backgrounds at each level of selection in dielectron channel, with statistical and systematic errors added in quadrature.

Category	Yield	Stat Err	Sys Err
$Z/\gamma^* \rightarrow \tau\tau$	0.15	0.05	$^{+0.05}_{-0.10}$
WW	0.14	0.01	$^{+0.08}_{-0.07}$
Fakes	0.91	0.22	0.20
Total Bkg	1.20	0.23	$^{+0.22}_{-0.23}$
Expected signal	1.39	0.04	$^{+0.16}_{-0.22}$
signal efficiency	0.078	± 0.002	$^{+0.009}_{-0.012}$
Selected Events	5		

TABLE III: Expected background and observed and expected signal yields in the $t\bar{t} \rightarrow ee$ channel. The expected signal yield assumes a 7 pb $t\bar{t}$ production cross section.

E. Dimuon channel

The preselection of candidate events in the dimuon channel is based on the following requirements:

- primary vertex with $N_{trk} > 2$ and $|vtx_z| < 60$ cm
- 2 isolated muons with track match, $P_T^\mu > 15$ GeV, opposite electrical charge, muon track originates from primary vertex $|\Delta z(e, PV)| < 1$ cm, $|dca|/\sigma_{dca} < 3$.
- muon trigger
- ≥ 2 jets with $P_T^j > 20$ GeV

Table IV summarizes the cut flow at the various stages of the event selection after the preselection in the $\mu\mu$ channel and Table V shows the final yield of background and signal events, the latter for the assumption of a $t\bar{t}$ production cross section of 7 pb.

Distributions of kinematic variables in the dimuon channel are shown in Appendix X.

Criteria	Data	Total	Fakes	Z/γ^*	WW	$t\bar{t}$
Preselection cuts	128	133.8 ± 26.0	7.68 ± 1.42	124.0 ± 25.9	0.276 ± 0.102	1.87 ± 0.34
$\Delta\phi(\mu_{leading}, \cancel{E}_T) < 165^\circ$ and $M_{\mu\mu}$ cuts	22	27.6 ± 4.8	3.66 ± 0.59	22.7 ± 4.8	0.199 ± 0.074	1.07 ± 0.20
$H_T^\mu > 120$ GeV cut	17	18.2 ± 3.1	2.49 ± 0.47	14.5 ± 3.1	0.152 ± 0.057	1.04 ± 0.19
$\cancel{E}_T > 35$ GeV cut	4	$3.44 \pm .55$	0.46 ± 0.20	2.04 ± 0.49	0.104 ± 0.040	0.83 ± 0.15

TABLE IV: Data, expected signal and backgrounds at each level of selection in dimuon channel. The errors are combined statistical and systematic, with the larger of the JES systematic error used.

Category	Yield	Stat Err	Sys Err
Z/γ^*	2.04	0.38	$+0.31$ -0.83
WW	0.10	0.02	0.02
Fakes	0.46	0.19	0.05
Total Bkg	2.61	0.43	$+0.31$ -0.83
Expected Signal	0.83	0.06	$+0.13$ -0.14
signal efficiency	0.054	± 0.004	$+0.008$ -0.009
Selected Events	4		

TABLE V: Expected background and observed and expected signal yields in the $t\bar{t} \rightarrow \mu\mu$ channel. The expected signal yield assumes a 7 pb $t\bar{t}$ production cross section.

F. Electron-muon channel

The preselection of candidate events in the electron-muon channel is based on the following requirements:

- primary vertex with $N_{trk} > 2$ and $|vtx_z| < 60$ cm
- 1 tight electron (based electron ID likelihood) with track match, originating from the primary vertex $|\Delta z(e, PV)| < 1$ cm
- 1 muon with track match, originating from the primary vertex $|\Delta z(\mu, PV)| < 1$ cm
- electron and muon trigger

Table VI summarizes the cut flow at the various stages of the event selection after the preselection in the $e\mu$ channel and Table VII shows the final yield of background and signal events, the latter for the assumption of a $t\bar{t}$ production cross section of 7 pb.

Distributions of kinematic variables in the dimuon channel are shown in Section X.

Cut	Data	Total	Fakes	$Z/\gamma^* \rightarrow ll + jets$		$WW \rightarrow e\mu$	$t\bar{t}$
				$Z/\gamma^* \rightarrow \tau\tau$	$Z/\gamma^* \rightarrow \mu\mu$		
One tight EM and one isolated muon with $\Delta R(e, \mu) > 0.25$	113	$110.79^{+6.70}_{-6.32}$	9.39 ± 2.91	$54.49^{+4.76}_{-4.33}$	$30.43^{+3.56}_{-3.39}$	$10.48^{+0.96}_{-1.01}$	$5.98^{+0.47}_{-0.48}$
$\cancel{E}_T > 25$ GeV	29	$23.80^{+2.17}_{-2.37}$	3.80 ± 1.18	$3.93^{+0.72}_{-0.81}$	$2.95^{+0.91}_{-0.95}$	$7.74^{+1.32}_{-1.58}$	$5.38^{+0.39}_{-0.44}$
Two jets with $p_T > 15$ GeV	10	$6.57^{+0.56}_{-0.54}$	0.49 ± 0.15	$0.95^{+0.34}_{-0.30}$		$0.67^{+0.12}_{-0.13}$	$4.45^{+0.38}_{-0.40}$
Two jets with $p_T > 20$ GeV	8	$5.65^{+0.51}_{-0.56}$	0.31 ± 0.09	$0.71^{+0.27}_{-0.23}$		$0.46^{+0.11}_{-0.11}$	$4.17^{+0.42}_{-0.49}$
$H_T^{leading\ lepton} > 140$ GeV	8	$4.73^{+0.46}_{-0.51}$	0.19 ± 0.06	$0.47^{+0.18}_{-0.16}$		$0.29^{+0.06}_{-0.06}$	$3.77^{+0.42}_{-0.47}$

TABLE VI: Data, expected signal and backgrounds at each level of selection in electron-muon channel, with statistical and systematical errors.

Category	Yield	Stat Err	Sys Err
$Z/\gamma^* \rightarrow \tau\tau$	0.47	0.11	$^{+0.14}_{-0.12}$
WW	0.29	0.00	0.06
Fakes	0.19	0.02	0.05
Total Bkg	0.95	± 0.11	$^{+0.16}_{-0.14}$
Expected Signal	3.77	0.08	$^{+0.41}_{-0.47}$
signal efficiency	0.117	± 0.005	$^{+0.015}_{-0.013}$
Selected Events	8		

TABLE VII: Expected background and observed and expected signal yields in the $e\mu$ channel. The expected signal yield assumes a 7 pb $t\bar{t}$ production cross section.

G. Combined plots for all three channels

Table VIII shows the final yield of background and signal events for the three dilepton channels, the latter for the assumption of a $t\bar{t}$ production cross section of 7 pb. Figure 1 shows kinematic distributions, combined for the three dilepton channels, after final event selection.

Figure 2 shows an event display of a candidate event in the $e\mu$ channel. Clearly visible are the high- P_T electron and muon, the latter leaving a MIP signal (Muon Tracking in the Calorimeter = MTC) in the calorimeter. Jet1 has a secondary vertex and jet2 has a soft-muon, both being indications for the jets to be b -jets.

Category	ee	$\mu\mu$	$e\mu$	ll
Z/γ^*	0.15 ± 0.10	2.04 ± 0.49	0.47 ± 0.17	2.66 ± 0.53
WW	0.14 ± 0.08	0.10 ± 0.04	0.29 ± 0.06	0.53 ± 0.11
Fakes	0.91 ± 0.30	0.46 ± 0.20	0.19 ± 0.06	1.56 ± 0.36
Total background	1.20 ± 0.33	2.61 ± 0.53	0.95 ± 0.19	4.76 ± 0.65
Expected signal	1.39 ± 0.19	0.83 ± 0.15	3.77 ± 0.44	5.99 ± 0.50
SM expectation	2.59 ± 0.38	3.44 ± 0.55	4.73 ± 0.49	10.76 ± 0.83
Selected events	5	4	8	17

TABLE VIII: Expected background and observed and expected signal yields. The expected signal yield assumes a 7 pb $t\bar{t}$ production cross section. The errors shown are the quadratic sum of the statistical and the systematic errors.

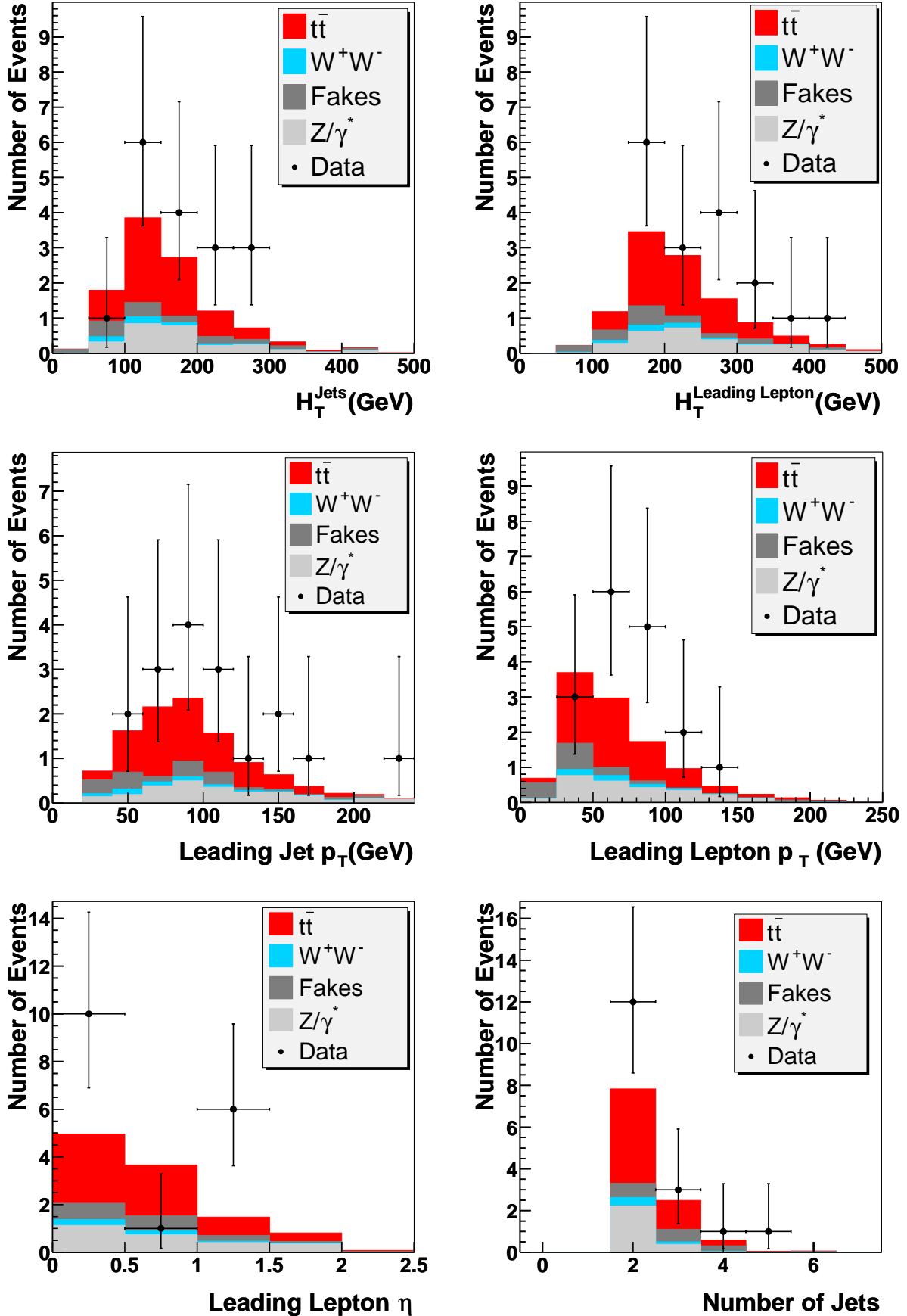


FIG. 1: Distribution of kinematic variables for the three dilepton channels combined. Top left: H_T^{jets} , Top right: H_T^{lepton} . Center left: leading jet p_T . Center right: leading lepton p_T . Bottom left: leading lepton η . Bottom right: Number of Jets.

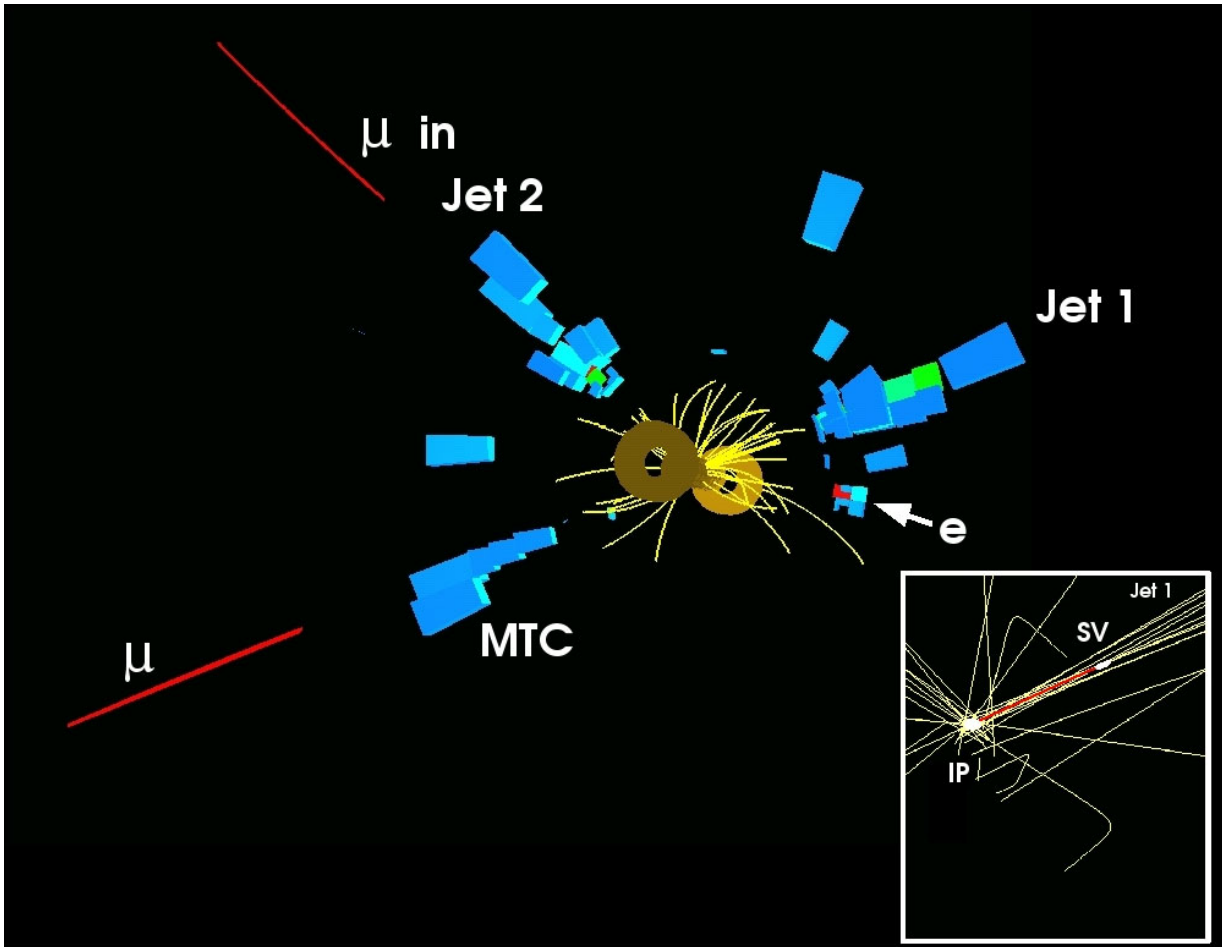


FIG. 2: Event display of a candidate event in the $e\mu$ channel. Clearly visible are the high- P_T electron and muon, the latter leaving a MIP signal (MTC) in the calorimeter. Jet1 has a secondary vertex and jet2 has a soft-muon, both being indications for the jets to be b -jets.

VI. SYSTEMATIC UNCERTAINTIES

Table IX summarizes the systematic uncertainties on the event selection efficiencies as determined from Monte Carlo. The Monte Carlo statistics uncertainties are treated as uncorrelated between channel, all other sources of systematic uncertainties are treated as correlated between channels. The jet energy scale uncertainty dominates the total systematic error.

source	$\mu\mu$	ee	$e\mu$
primary vertex	0.9%	0.8%	0.7%
EM reco		3%	1.5%
EM ID		0.2%	0.1%
EM tracking		0.7%	0.3%
EM likelihood		1.2%	0.5%
L1 EM trigger		0.1%	(+1.1 – 1.0)%
L2 EM trigger			
L3 EM trigger		0.3%	(+0.6 – 0.7)%
μ ID	3%		1.6%
μ isolation	6%		3%
$\mu \sigma_{dca}$	4.4%		2.2%
μ tracking	4%		2%
χ^2	2%		1%
L1 μ trigger	1%		(+2.3 – 2.8)%
L2 μ trigger			
L3 μ trigger			
Δz	1%	1%	1%
JES	(+6 – 10)%	(+5.8 – 8.0)%	(+7.1 – 9.5)%
Jet ID	–6.2%	–7.3%	–4.1%
Jet resolution	2%	1.0%	2.2%
multi parton interaction	1.2%	4.2%	2.3%
top mass	6%	(+3.5 – 6.4)%	4%
uncorrelated	7%	3%	4%

TABLE IX: Summary of the relative systematic uncertainties on the $t\bar{t} \rightarrow \ell\bar{\ell}$ signal efficiencies.

Table X summarizes the systematic uncertainties on the background estimates as determined from Monte Carlo or from data. The Monte Carlo statistics, the fake rate uncertainties and the scale factor uncertainties are added in quadrature and treated as uncorrelated between channels, all other sources of systematic uncertainties are treated as correlated between channels. The jet energy scale uncertainty along with the uncertainty on the LO to NLO scale factor of the WW cross section and the uncertainty on the Z background normalization, originating from studies on the jet p_T spectra in $(Z/\gamma^* \rightarrow ll)jj$ events dominate the total systematic uncertainties.

VII. CROSS SECTIONS

The $t\bar{t}$ cross section is measured by maximizing the product of the likelihoods for each individual channel, based on the Poisson probability to observe a given number of events under the signal-plus-background hypothesis.

The number of observed events, the estimated background, the $t\bar{t}$ selection efficiency, the decay branching ratio for $t\bar{t} \rightarrow ll' + X$ decays, including the $W \rightarrow \tau\nu \rightarrow (e, \mu)\nu\nu$ contribution, as derived from [8], and the integrated luminosity for each channel are summarized in Table XI.

The resulting likelihoods as a function of the $t\bar{t}$ production cross section for the three separate channels and for the combination are shown in Section IX

The systematic uncertainty on the cross section measurement is obtained by varying the background and efficiencies, within their errors, with all the correlations between the channels and between the different classes of background taken into account. Uncertainties from limited Monte Carlo statistics and from fake background are treated as uncorrelated.

channel	ee		$e\mu$		$\mu\mu$	
source	WW	$Z \rightarrow \tau\tau$	WW	$Z \rightarrow \tau\tau$	WW	$Z/\gamma^* \rightarrow \mu\mu$
primary vertex	0.8%	0.8%	0.7%	0.7%		
EM reco	3%	3%	1.5%	1.5%		
EM ID	0.2%	0.2%	0.1%	0.1%		
EM tracking	0.7%	0.7%	0.3%	0.3%		
EM likelihood	1.2%	1.2%	0.5%	0.5%		
L1 EM trigger	0.1%	1.7%	(+1.1 – 1.0)%	(+3.3 – 1.0)%		
L2 EM trigger						
L3 EM trigger	0.3%	2.3%	(+0.6 – 0.7)%	(+0.8 – 2.3)%		
μ ID			1.6%	1.6%	3%	
μ isolation			3%	3%	6%	
$\mu \sigma_{dca}$			2.2%	2.2%	4.4%	
μ tracking			1.0%	1.0%	4%	
χ^2			1%	1%	2%	
L1 μ trigger			(+3.6 – 4.5)%	(+4.5 – 3.5)%	1%	
L2 μ trigger						
L3 μ trigger						
Δz	1%	1%	1%	1%	1%	
JES	(+44.2 – 22.1)%	(+25.0 – 50.0)%	(+22.6 – 15.2)%	(+27.3 – 23.6)%	(+31.7 – 22.1)%	(+15.0 – 3.6)%
Jet ID	-16.7%	-16.7%	-7.4%	-7.4%	-6.2%	
Jet resolution	17%	20%	2.5%	2.5%	2%	
Z background		-40%		-40%		-40%
WW cross section	35%		35%		35%	
uncorrelated	25%		13%		16%	

TABLE X: Summary of the relative systematic uncertainties on background.

Channel	nr. obs. events	backgrd	$\epsilon_{t\bar{t}}$	Br	\mathcal{L} (pb $^{-1}$)
ee	5	1.20	0.078	0.01631	156.33
$\mu\mu$	4	2.61	0.054	0.01581	139.58
$e\mu$	8	0.95	0.117	0.03212	142.73

TABLE XI: Number of observed events, estimated background, $t\bar{t}$ selection efficiency, decay branching ratio for $t\bar{t} \rightarrow l\bar{l} + X$ including the $W \rightarrow \tau\nu \rightarrow (e, \mu)\nu\nu$ contribution, and integrated luminosity for each channel.

The preliminary $t\bar{t}$ production cross sections at $\sqrt{s} = 1.96$ TeV in dilepton channels are measured to be (see Figure 3):

$$ee : \quad \sigma_{t\bar{t}} = 19.1_{-9.6}^{+13.0} \text{ (stat)} \quad {}_{-2.6}^{+3.7} \text{ (syst)} \pm 1.2 \text{ (lumi) pb;} \quad (1)$$

$$\mu\mu : \quad \sigma_{t\bar{t}} = 11.7_{-14.1}^{+19.7} \text{ (stat)} \quad {}_{-5.0}^{+7.9} \text{ (syst)} \pm 0.8 \text{ (lumi) pb;} \quad (2)$$

$$e\mu : \quad \sigma_{t\bar{t}} = 13.1_{-4.7}^{+5.9} \text{ (stat)} \quad {}_{-1.7}^{+2.2} \text{ (syst)} \pm 0.9 \text{ (lumi) pb;} \quad (3)$$

$$\text{dilepton} : \quad \sigma_{t\bar{t}} = 14.3_{-4.3}^{+5.1} \text{ (stat)} \quad {}_{-1.9}^{+2.6} \text{ (syst)} \pm 0.9 \text{ (lumi) pb.} \quad (4)$$

VIII. CONCLUSION

A measurement of the $t\bar{t}$ cross section at the Tevatron at $\sqrt{s} = 1.96$ TeV has been performed in the three dilepton channels (ee , $e\mu$, and $\mu\mu$). The individual results of each analysis are summarized in Equations 1 to 3 and Figure 3. The combined result, which is shown in Figures 3 and 4, yields

$$\text{dilepton} : \quad \sigma_{t\bar{t}} = 14.3_{-4.3}^{+5.1} \text{ (stat)} \quad {}_{-1.9}^{+2.6} \text{ (syst)} \pm 0.9 \text{ (lumi) pb.}$$

[1] ‘THE $t\bar{t}$ CROSS-SECTION AT 1.8 AND 1.96 TEV: A STUDY OF THE SYSTEMATICS DUE TO PARTON DENSITIES AND SCALE DEPENDENCE’, M. Cacciari et al., hep-ph/0303085.

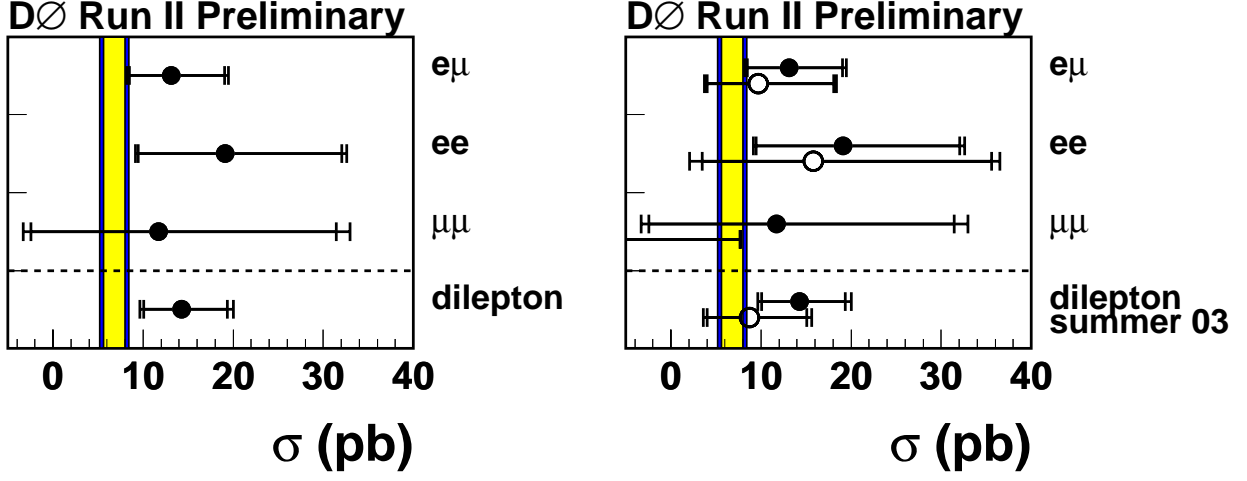


FIG. 3: Preliminary $t\bar{t}$ production cross section as measured in the dilepton channels compared to the corresponding results from the summer 2003 and theoretical calculations by Kidonakis (inner yellow band, hep-ph/0303186) and Cacciari et al. (outer blue band, hep-ph/0303085).

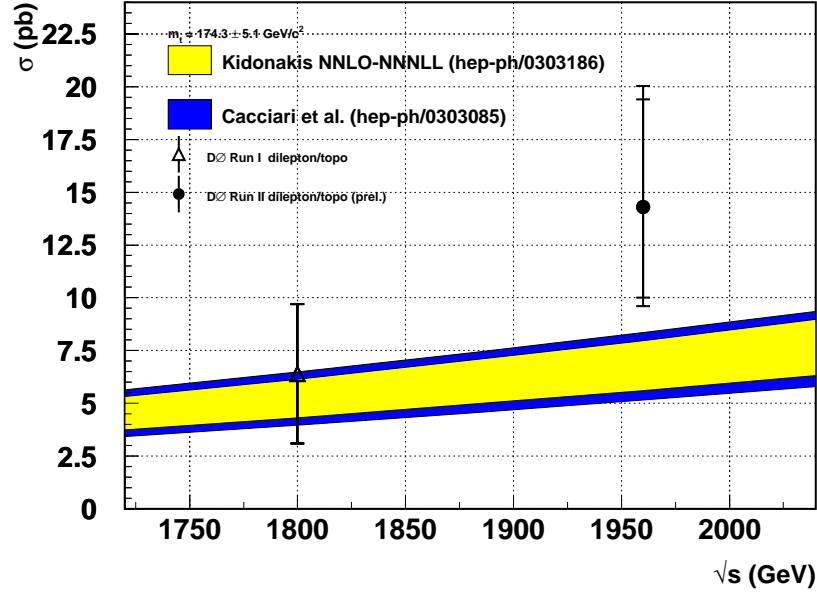


FIG. 4: Preliminary $t\bar{t}$ production cross section as measured in the dilepton channels compared to the corresponding results from Run-I and theoretical calculations by Kidonakis (inner yellow band, hep-ph/0303186) and Cacciari et al. (outer blue band, hep-ph/0303085).

- [2] 'A unified approach to NNLO soft and virtual corrections in electroweak, Higgs, QCD and SUSY processes', N. Kidonakis, hep-ph/0303186.
- [3] ALPGEN, a generator for hard multiparton processes in hadronic collisions, M.L. Mangano et al., JHEP 0307:001, 2003, hep-ph/0206293.
- [4] New Generation of Patron Distributions with Uncertainties from Global QCD Analysis, CTEQ6, hep-ph/0201195.
- [5] PYTHIA 6.2, Physics and Manual, T. Sjöstrand et al., LU TP 01-21, hep-ph/0108264.
- [6] DØ Electroweak Physics Group
http://www-d0.fnal.gov/Run2Physics/wz/Public/results/r2zmumucs_summer03.html
- [7] J.M. Campbell and R.K. Ellis, Phys.Rev.D **60** (1999) 113006.
- [8] The Review of Particle Physics, K. Hagiwara et al., Phys. Rev. D**66**, 010001 (2002).

IX. APPENDIX A: $t\bar{t}$ CROSS SECTION LIKELIHOOD CURVES

The resulting likelihoods as a function of the $t\bar{t}$ production cross section for the three separate channels and for the combination are shown in Figure 5.

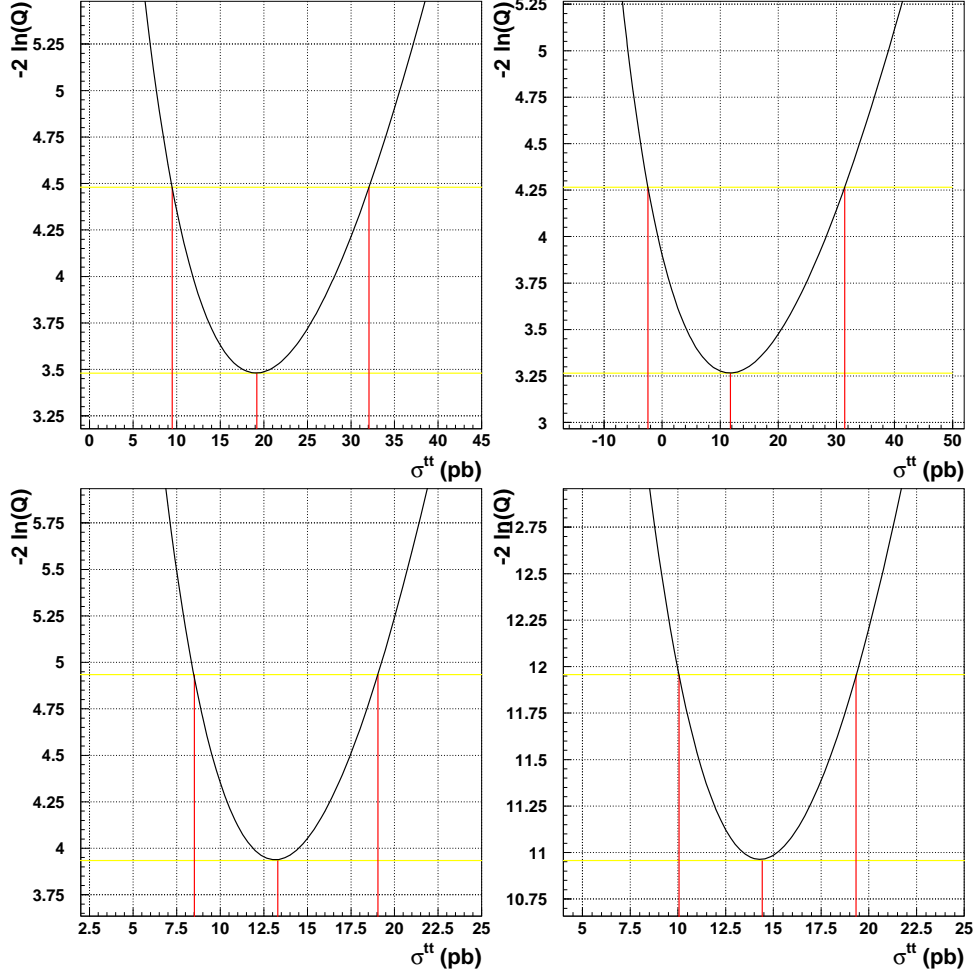


FIG. 5: Likelihood as a function of the $t\bar{t}$ production cross section. The central value and the statistical errors are indicated as vertical line. Top left: Dielectron channel; Top right: Dimuon channel; Bottom left: $e\mu$ channel; Bottom right: Dilepton channels combined.

X. APPENDIX B: SINGLE CHANNEL KINEMATIC DISTRIBUTIONS

Figure 6 shows the distribution of \cancel{E}_T versus M_{ee} after preselection cuts in the dielectron channel.

Figure 7 shows distributions of kinematic variables of the dielectron candidate events after lepton P_T and \cancel{E}_T cuts, and Figure 8 after the final event selection cuts.

Figure 9 shows the distribution of \cancel{E}_T versus $M_{\mu\mu}$ after preselection cuts in the dimuon channel.

Figure 10 shows distributions of kinematic variables of the dimuon candidate events after the preselection cuts, and Figure 11 after the final event selection cuts.

Figure 12 shows the \cancel{E}_T distribution after the preselection and the number of jets after the preselection and the $\cancel{E}_T > 25$ GeV cut in the $e\mu$ channel.

Figure 13 shows distributions of kinematic variables of the $e\mu$ candidate events after the final event selection cuts.

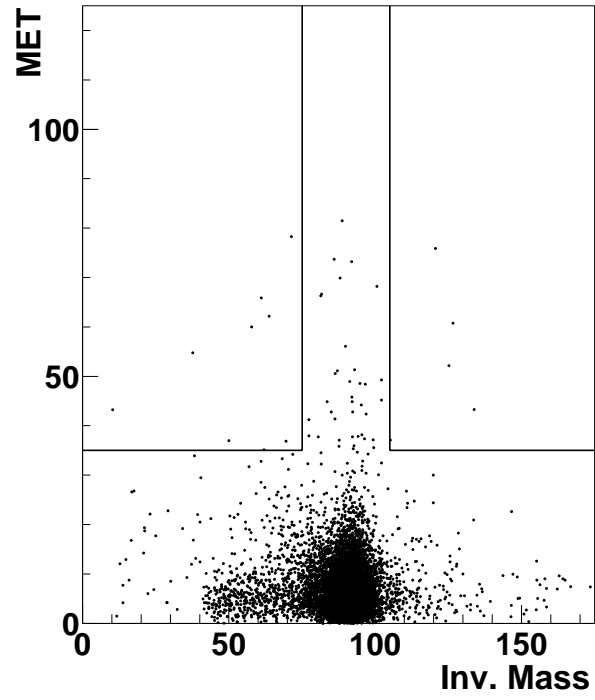


FIG. 6: \cancel{E}_T vs. M_{ee} distribution after preselection cuts. Also shown is the applied cut.

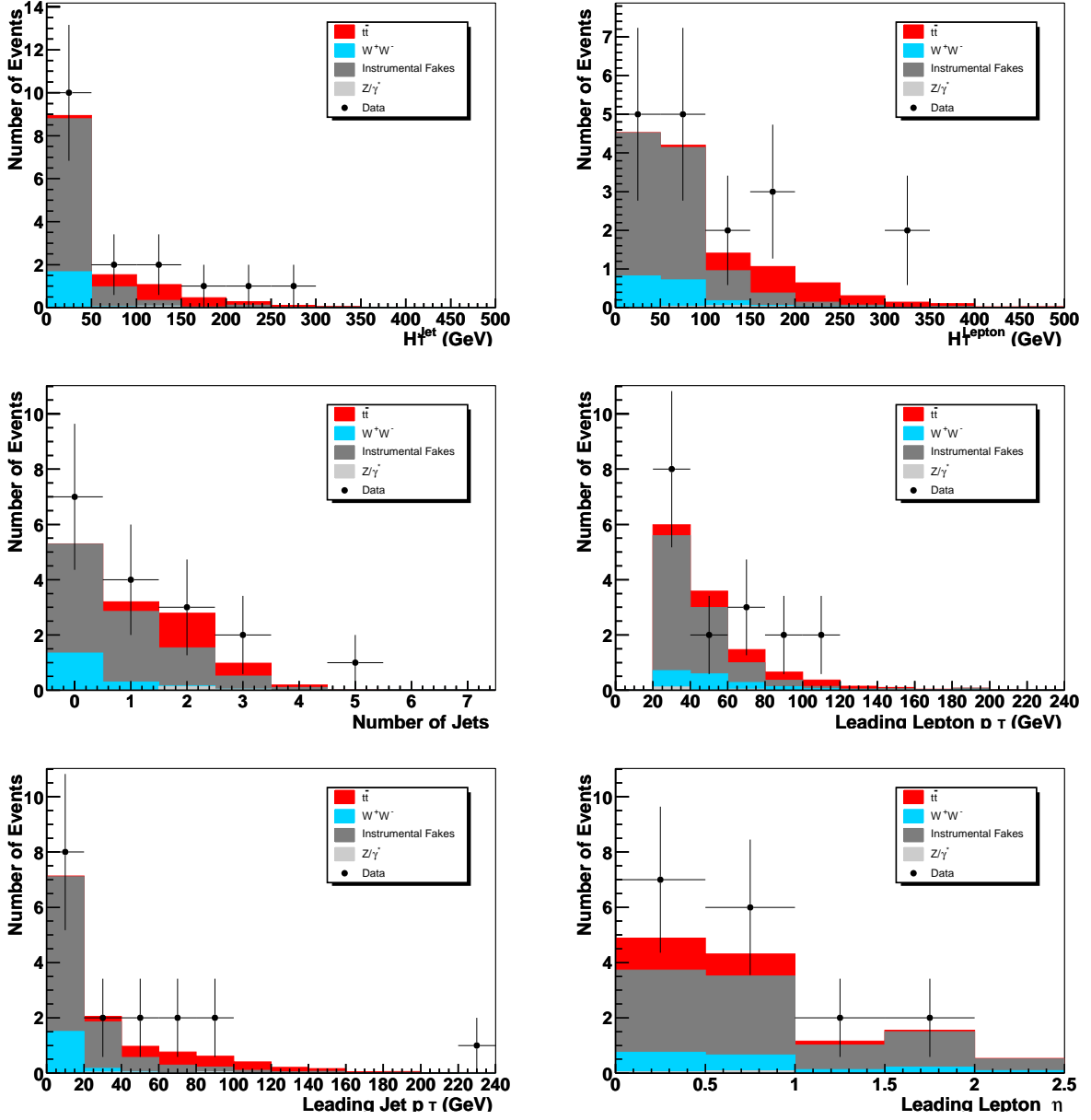


FIG. 7: Distribution of kinematic variables in the dielectron channel after lepton p_T and \cancel{E}_T cuts. Top left: H_T^{jet} , Top right: H_T^{lepton} , Center left: Number of jets, Center right: leading lepton p_T , Bottom left: leading jet p_T , Bottom right: leading electron η .

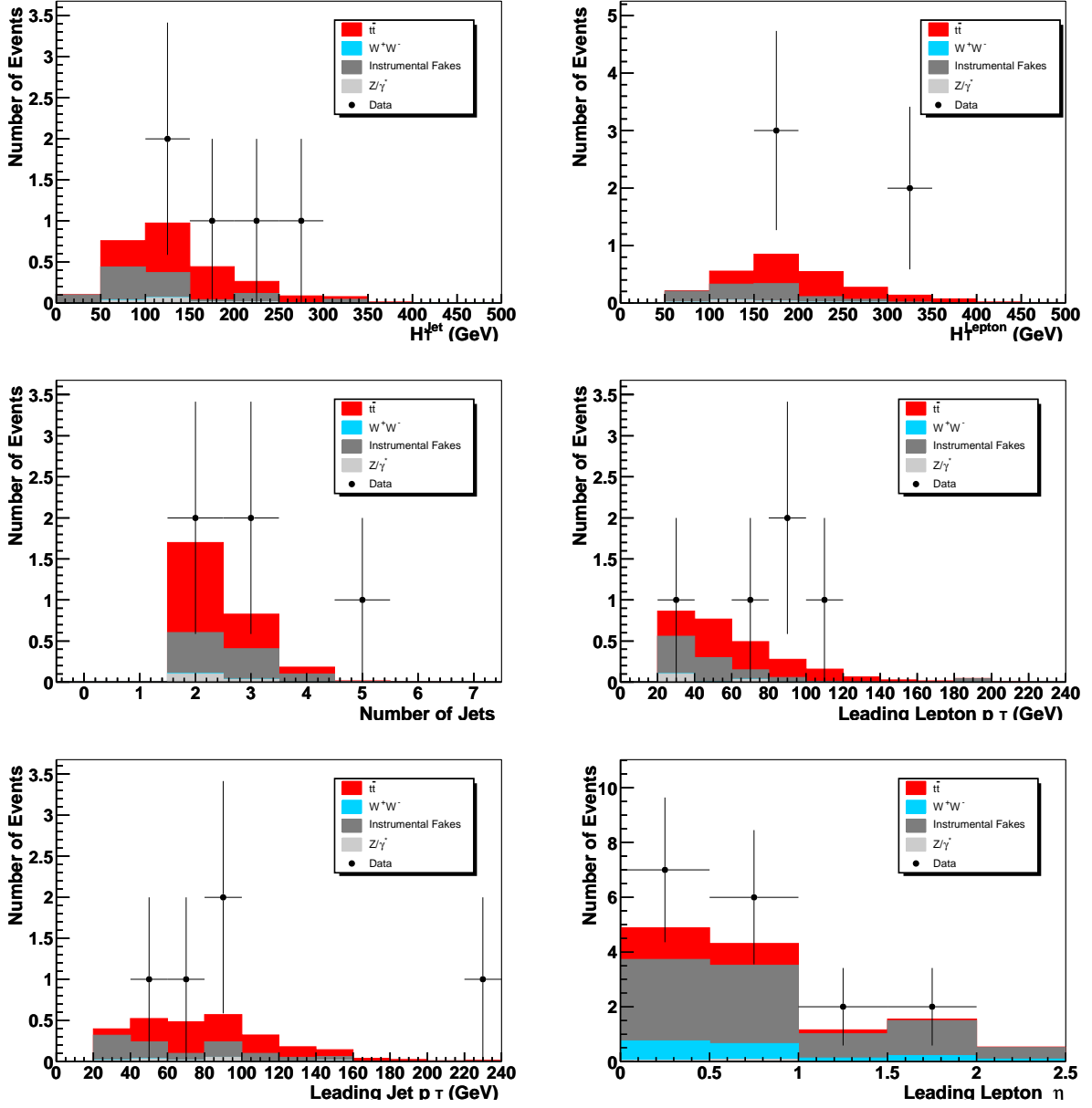


FIG. 8: Distribution of kinematic variables in the dielectron channel after final selection cuts. Top left: H_T^{jet} , Top right: H_T^{lepton} , Center left: Number of jets, Center right: leading lepton p_T , Bottom left: leading jet p_T , Bottom right: leading electron η .

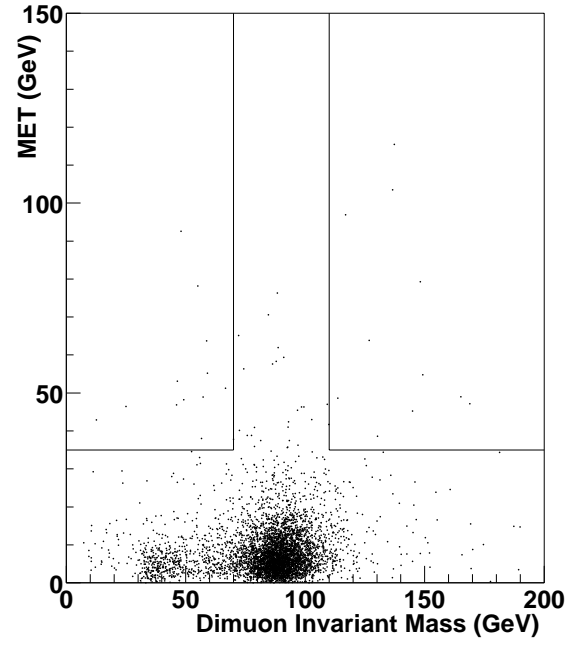


FIG. 9: \cancel{E}_T vs. $M_{\mu\mu}$ distribution in data events passing the dimuon preselection criteria. The lines indicate the cut values of $\cancel{E}_T > 35$ GeV and $M_{\mu\mu} < 70$ GeV or > 110 GeV.

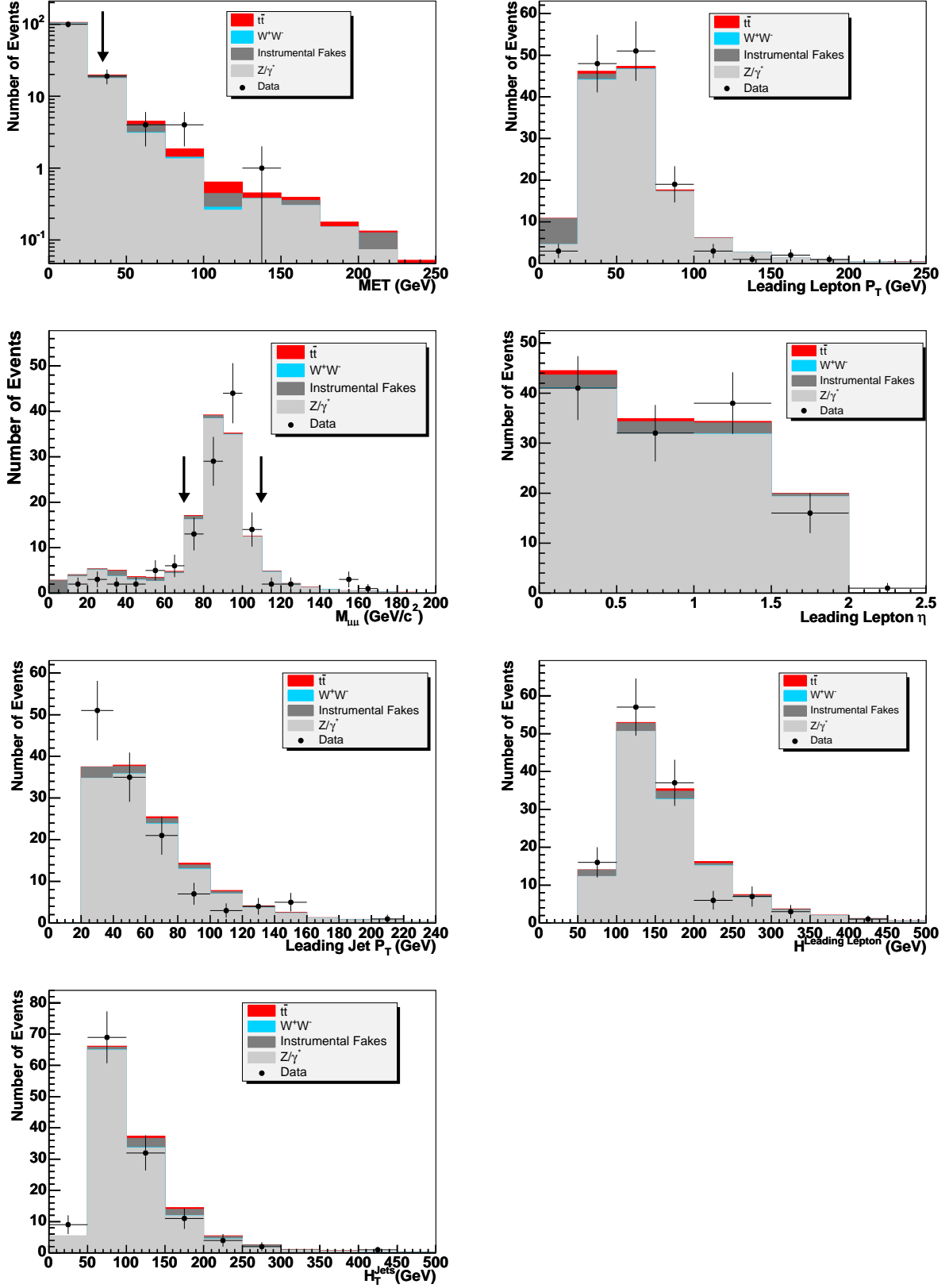


FIG. 10: Distribution of kinematic variables in the dimuon channel after preselection cuts. Top left: \cancel{E}_T , Top right: leading muon p_T , Center left: dimuon mass, Center right: leading muon η , Bottom left: leading jet p_T , Bottom right: H_T^μ , Bottom most left: H_T^{jets} .

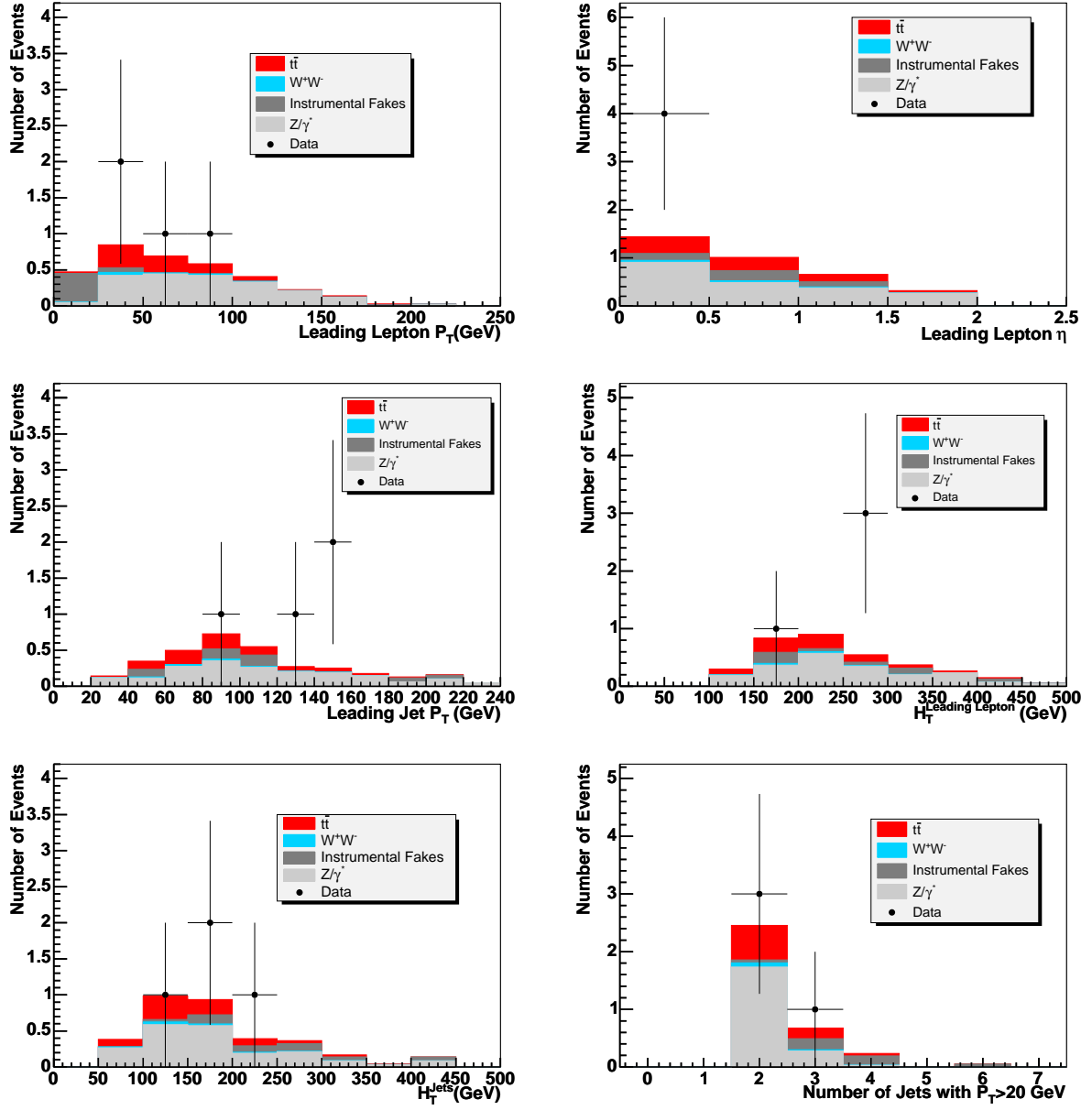


FIG. 11: Distribution of kinematic variables in the dimuon channel after final selection cuts. Top left: leading muon p_T , Top right: leading muon η , Center left: leading jet p_T , Center right: H_T^μ , Bottom left: H_T^{jets} , Bottom right: number of jets.

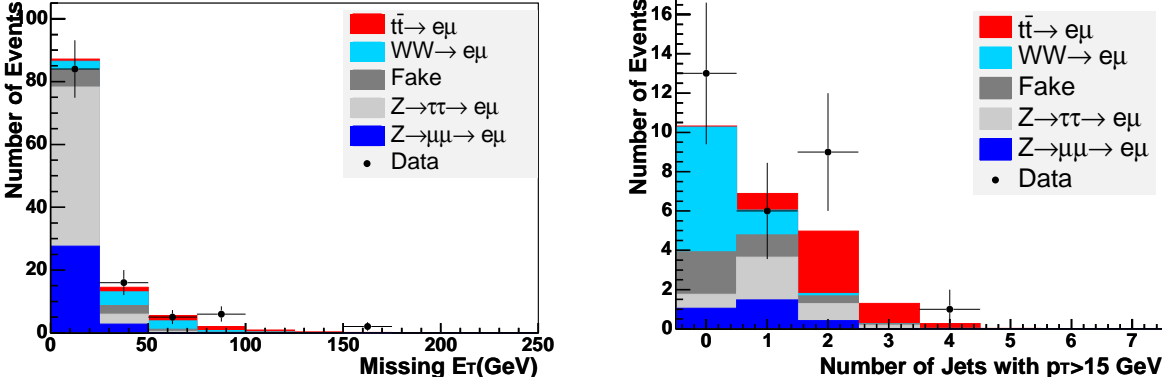


FIG. 12: Distribution of kinematic variables in the $e\mu$ channel. Left: \cancel{E}_T after the preselection; Right: number of jets after preselection and the $\cancel{E}_T > 25$ GeV cut.

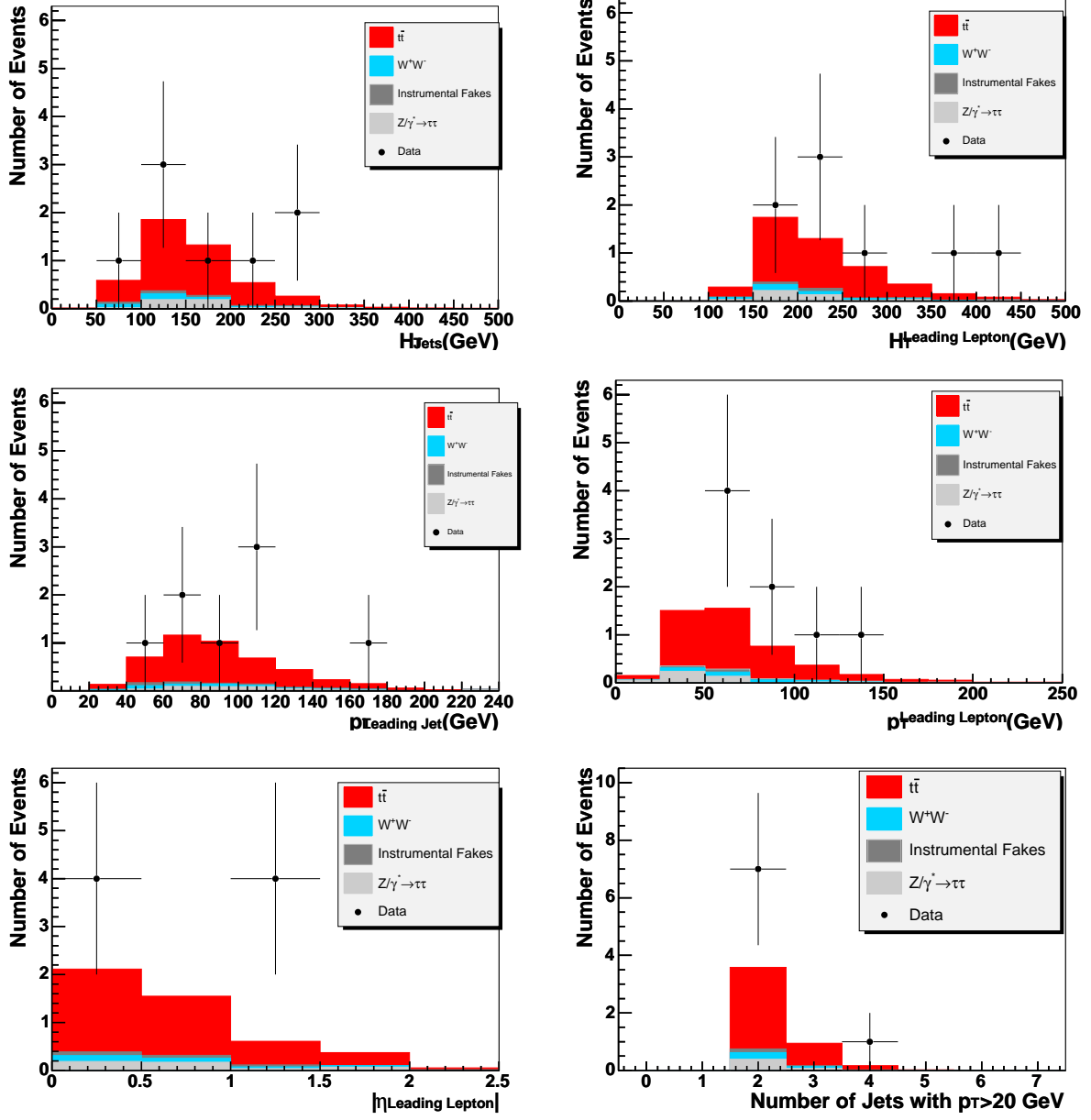


FIG. 13: Distribution of kinematic variables in the $e\mu$ channel after final selection cuts. Top left: H_T^{jets} , Top right: H_T^{lepton} , Center left: leading jet p_T , Center right: leading lepton p_T , Bottom left: leading lepton η , Bottom right: number of jets.